NASA Contractor Report 187078

The Role of Gravity on Macrosegregation in Alloys

D.R. Poirier, C.F. Chen, and J.C. Heinrich
The University of Arizona
Tuscon, Arizona

March 1991

NASA

THE ROLE OF GRAVITY ON MACROSEGREGATION IN ALLOYS

D.R. Poirier, C.F. Chen, and J.C. Heinrich
The University of Arizona
College of Engineering and Mines
Tucson, Arizona 85721

SUMMARY

During dendritic solidification liquid flow is induced both by buoyancy forces and solidification shrinkage. Based largely on the experimental base of other NASA-sponsored investigators, there is strong evidence that the major reason for the liquid flow is the former, i.e., thermosolutal convection. In the microgravity environment, it is thought that the thermosolutal convection will be greatly diminished so that convection will be confined mainly to the flow of interdendritic liquid required to satisfy the solidification shrinkage.

The major motivation for this work has been to provide improved models to the NASA community involved in performing and planning space experiments on dendritic solidification with emphasis on convection and macrosegregation. Another motivation for this work is that macrosegregation is an extremely important subject to the commercial casting community. We believe that work of this type, especially when combined with the experimental results of other NASA-sponsored investigators, will be crucially important in providing a basic understanding of macrosegregation to the casting community.

This report describes the simulation of thermosolutal convection in directionally solidified (DS) alloys. A linear stability analysis was used to predict marginal stability curves for a system that comprises a mushy zone underlying an all-liquid zone. In the unperturbed and nonconvecting state (i.e., the basic state), isotherms and isoconcentrates

are planar and horizontal. The mushy zone is realistically treated as a medium with a variable volume fraction of liquid that is consistent with the energy and solute conservation equations. The perturbed variables include temperature, concentration of solute, and both components of velocity in a two-dimensional system. As a model system, an alloy of Pb-20 wt pct Sn, solidifying at a velocity of 2 x 10^{-3} cm·s^{-1}, was selected. Dimensional numerical calculations were done to define the marginal stability curves in terms of the thermal gradient at the dendrite tips, G_L, vs the horizontal wave number of the perturbed quantities. For a gravitational constant of 0.01 $g_0 \leq g \leq g_0$, (g_0 = 9.8 cm·s^{-2}), the marginal stability curves show no minima; thus, the system is never unconditionally stable. Nevertheless, such calculations quantify the effect of reducing the gravitational constant on reducing convection and suggest lateral dimensions of the mold for the purpose of suppressing convection. Finally, for a gravitational constant of $10^{-4} g_0$, calculations show that the system is stable for the thermal gradients investigated (2.5 $\leq G_L \leq$ 100 K·cm^{-1}).

The supercritical thermosolutal convection in directionally solidified dendritic alloys was also modeled. The model assumes a nonconvective initial state with planar and horizontal isotherms and isococentrates that move upward at a constant solidification velocity. The initial state is perturbed, nonlinear calculations are performed to model convection of the liquid when the system is unstable, and the results are compared with the predictions of a linear stability analysis. The mushy zone is modeled as a porous medium of variable porosity, consistent with the volume fraction of interdendritic liquid that satisfies the conservation equations of energy and solute concentrations. Results are presented for systems involving lead-tin alloys (Pb-10 wt pct

Sn and Pb-20 wt pct Sn) and show significant differences with results of plane-front solidification. The calculations show that convection in the mushy zone is mainly driven by convection in the all-liquid region, and convection of the interdendritic liquid is only significant in the upper 20 pct of the mushy zone if it is significant at all. The calculated results also show that the systems are stable at reduced gravity levels of the order of $10^{-4} g_0$ or when the lateral dimensions of the container are small enough, for stable temperature gradients between $2.5 \leq G_L \leq 100$ K$\cdot$cm^{-1} at solidification velocities of 2 to 8 cm$\cdot$h^{-1}.

The linear stability analyses and the calculations of the nonlinear thermosolutal convection can be used to study the dendritic solidification. In addition to those tasks, this report briefly describes analysis and experiments on thermal and salt-finger convection in systems comprising a fluid layer overlying a porous medium. Finally, the aspect of solute redistribution during dendritic solidification was extended in a model to predict the formation of microporosity. Lacking data pertaining to the solidification of alloys, methods to estimate necessary transport and thermodynamic properties were also developed.
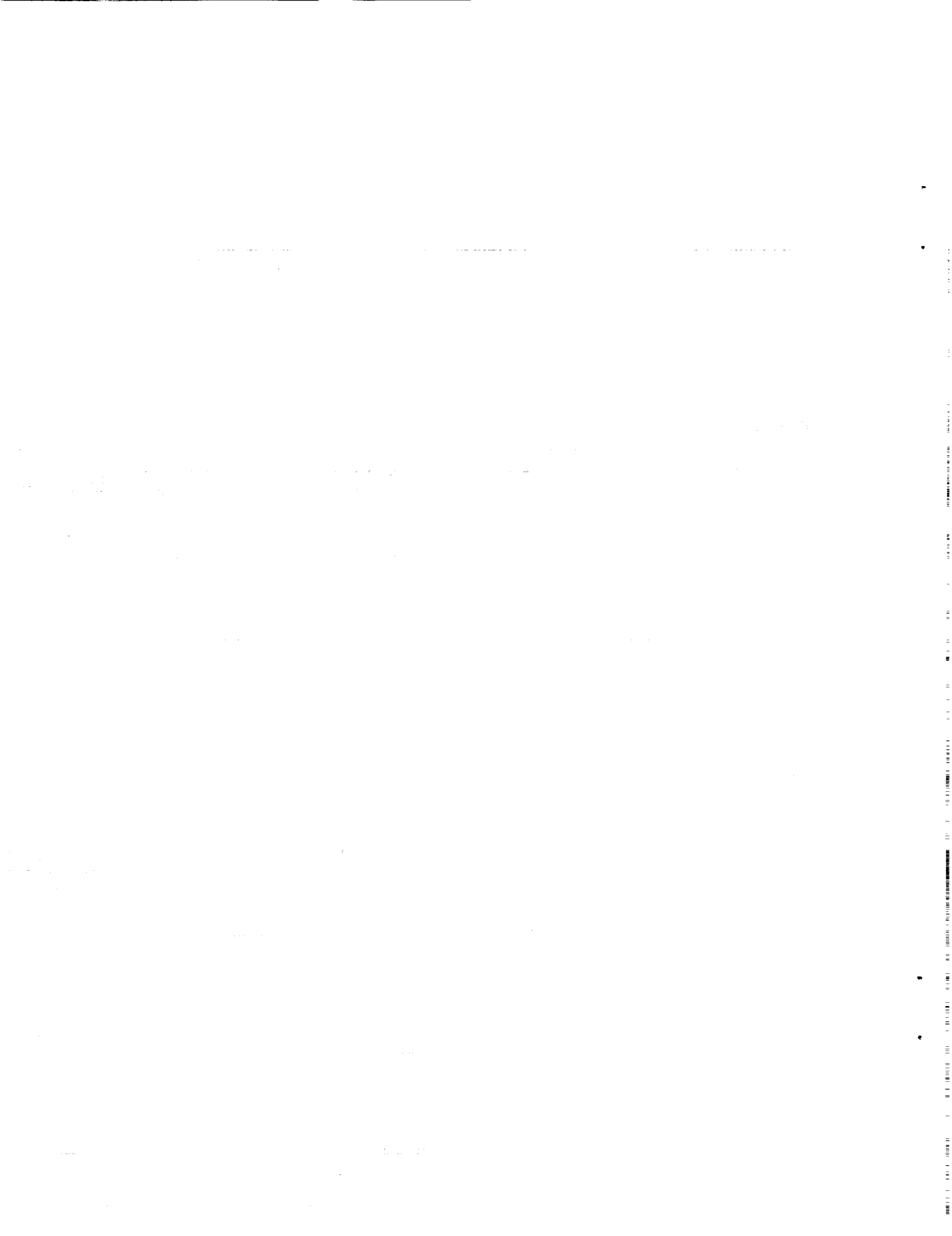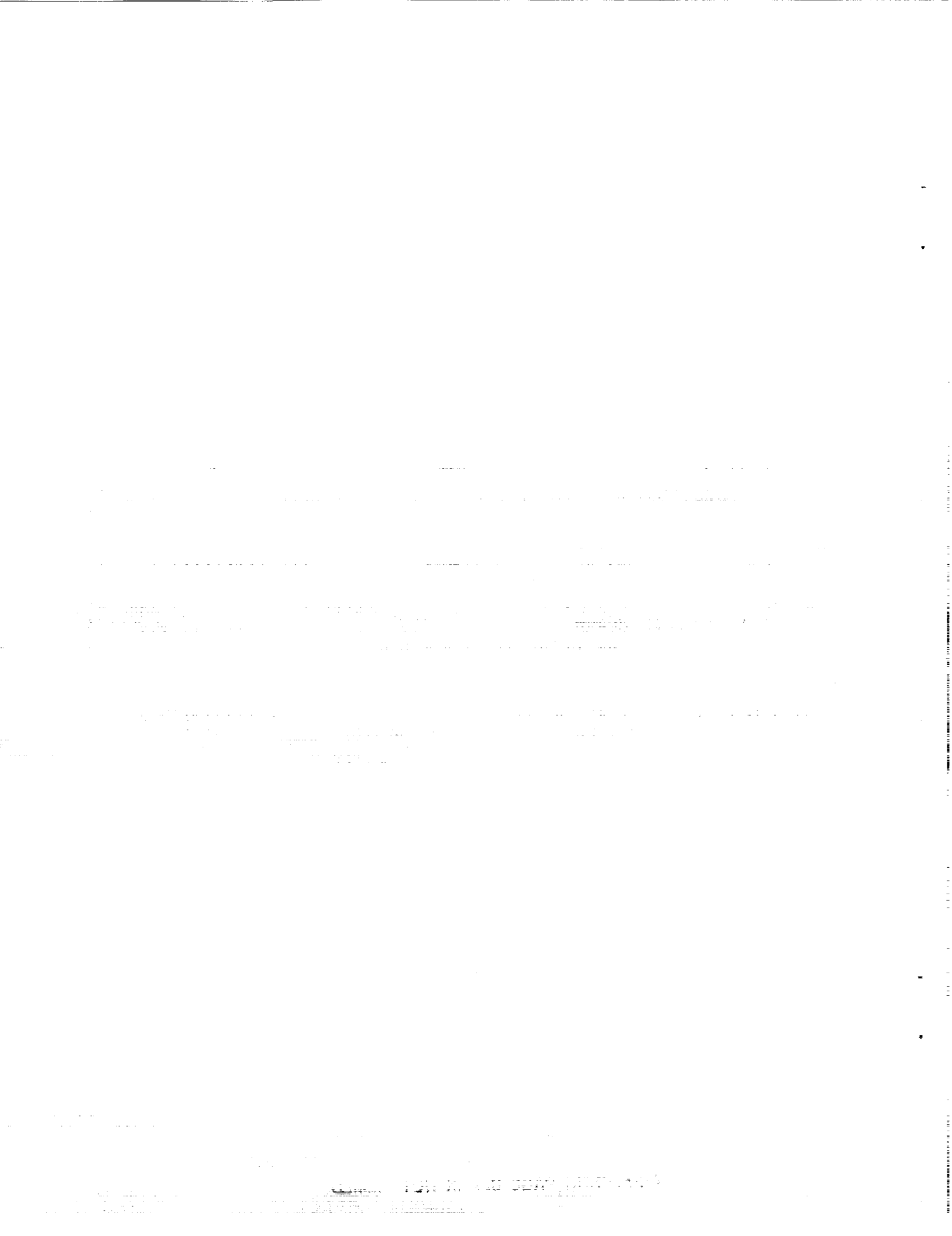
TABLE OF CONTENTS

I. INTRODUCTION

The convection of interdendritic liquid in the solid plus liquid region of solidifying alloys is responsible for many types of macrosegregation in castings and ingots. The modeling of such convection and of the resulting macrosegregation has been the subject of many studies since about 1970. However, there are still some important aspects of convective phenomena that have not yet been incorporated into dendritic solidification theory. In this report, we tie together some fundamental aspects of dendritic solidification and of convection in order to model macrosegregation.

The susceptibility of cast alloys to macrosegregation is dealt with on a day-to-day basis by foundrymen, ingot-makers and continuous casting engineers alike. For the most part, the approach to solving macrosegregation problems is to evaluate a number of full-scale production runs to determine acceptable processing parameters for each new alloy. While segregation is sometimes reduced by these empirical methods, it usually persists, and often is found to reach unacceptable levels leading to expensive scrap. In many processes, macrosegregation in castings, ingots or billets is the overriding factor in limiting the size and production rate of the cast product.

In terms of applications, this report addresses the solidification of directionally solidified (DS) castings under conditions in which thermosolutal convection is important. During the grant period, we did both linear and nonlinear calculations to predict the conditions for the onset of convective instability and to predict the transient nature of the convection during the solidification of dendritic alloys.

Such numerical research can be used in support of NASA experiments designed to investigate convective phenomena and macrosegregation in dendritic alloys. In addition

1

to providing an analytical model for the dendritic solidification experiments, numerical models for solidification can be used to explore the effect of different orientations of the gravity vector on convection and macrosegregation in dendritically solidified alloys in the low-g environment.

II. MACROSEGREGATION AND THERMOSOLUTAL CONVECTION

A. *Early Analyses of Macrosegregation*

In the early works,[1-17] emphasis was on the description of solute redistribution, including convection of the interdendritic liquid, and macrosegregation; however, thermosolutal convection in the liquid was ignored. It was recognized that because of constitutional and thermal effects, the density of the interdendritic liquid varies, spatially and temporally within the mushy zone, so convection of the interdendritic liquid was predicted and calculated. The first model which included gravity-driven convection of interdendritic liquid was done by Mehrabian et al. in 1970.[5] That basic approach, with physical and numerical improvements, was subsequently used to model and study macrosegregation in cylindrical remelted ingots,[7-9,11-13,15] under thermal conditions in which the width of the mushy zone varied[10,14] and for multicomponent alloys.[10,12] But in all cases thermosolutal convection was neglected.

An example of the quantitative results obtained from one of the early studies is shown in Figure 1 in which the convection is relatively extensive. Figure 1a shows the positions and shapes of the liquidus and solidus isotherms in a cylindrical ingot. Because the isotherms are concave with respect to the all-liquid region, convection is downward and toward the center where the streamlines meet and then point upward (Figure 1b).

2

The solute-rich interdendritic liquid flows to the center; consequently macrosegregation is strongly positive (i.e., enriched in solute) at that location (Figure 1c). In Fig. 1b the streamlines, of course, do not terminate along the surface of the liquidus isotherm in an actual ingot. In the analysis used at the time (1977), convection in the all-liquid zone was ignored. Pressure on the liquidus surface was simply given as ambient pressure plus the metallostatic pressure, and this was used as a boundary condition for the pressure and velocity fields within the mushy zone, itself. Darcy's law was used to represent conservation of momentum in the mushy zone. This treatment is sufficient to describe macrosegregation when thermosolutal convection is not important and when the geometry of the mushy zone is prescribed.

Figure 1 is an example in which the segregation is in the form of a continuous variation in composition from surface-to-center. Another important manifestation of flow of interdendritic liquid is the formation of severe localized segregates, which are called "channel-segregates" or "freckles". Freckles were shown (by experiment and by calculation) to form when the solidification rate is relatively slow and the interdendritic liquid flows in the same direction as and faster than the isotherms. This causes a local remelting within the S/L zone and the formation of the channel-type segregates.[7-10,15,16]

B. *Thermosolutal Convection*

We emphasize that this reports deals with dendritic alloys. However, practically all of the published work pertaining to the analysis of thermosolutal convection in solidifying metals deals with "plane-front" processes in which the solid-liquid interface is nominally flat. Thus is terms of applications, the available literature is pertinent to crystal growing.

3

Nevertheless, as a starting point to this discussion, reference is made to this body of literature.

It is well known that during the plane front solidification of a binary alloy convective as well as morphological instabilities can set in due to thermosolutal effects.[18,19] The problem of morphological instability (in the absence of convection) was first considered by Tillers et al.[20] and later by Mullins and Sekerka.[21] It is further known that the morphologically unstable plane front may later evolve into a dendritic network.[22-24] The evolution of the morphologically unstable solidifying front into primary dendrites is qualitatively understood. However, the precise development of the dendritic network is still being actively investigated.

In addition to the morphological instability a convective instability has been shown to occur during crystal growth processes; the analysis of this mode was first performed by Coriell et al.[25] Their results for Pb-Sn alloys indicate that at low growth velocities the preferred instability is, in fact, the convective mode, which could give rise to a nonplanar interface and certainly to a solid of nonuniform composition. Their basic analysis was recently improved upon, by coupling the convective flow with the morphological instability. This was done by Coriell et al.[26] and by Brattkus and Davis.[27]

The convection which occurs during plane front solidification is the result of the interaction of a thermal gradient and a solutal gradient, often deemed doubly diffusive convection.[28] In the literature many studies have been reported on doubly diffusive systems showing the development of different types of motions such as finger convection, cellular convection, etc. depending upon the directions and the magnitude of thermal and the solutal gradients; for a review see Turner.[29] The research mentioned so far

4

considers the onset of various kind of instabilities. However, the theory is not developed well enough to predict the transitions toward the long term behavior of the system. For example, it is observed experimentally that during solidification of binary alloys, the dendritic network is a common occurrence, and the theories developed for solidification with a nominally plane front interface are not applicable to predicting convective instabilities in dendritic alloys.

It is well understood that microsegregation of solute is coincidental with the formation of dendrites. These effects are further coupled with convection of the interdendritic liquid, and this results in macrosegregation. Macrosegregation can be in the form of a freckle or channel-segregate and can occur in a directionally solidified casting [30]. Experimental investigations on Pb-Sn and NH_4Cl-H_2O systems have revealed that the formation of the channel-segregates is sometimes intimately related to convection in the all-liquid zones.[31,32]

Hills et al.[33] developed a full set of thermodynamic equations for the mushy zone. Huppert and Worster[34] also formulated a simple mathematical model for the mushy zone based on the principles of global conservation relationships. However, their model assumes a spatially uniform and temporally constant volume fraction of solid in the mushy zone and is not realistic for the case of alloy solidification. In a later study, Worster[35] proposed a model for the development of the mushy zone with time. However, his model neglects convection completely, and considers only the mass and energy equations. Other studies in the literature on the dynamic behavior of the mushy zone include papers by Ridder et al.[9,13] and Maples and Poirier.[14,21] The primary claim of these analyses was to calculate the macrosegregation. Yeum and Poirier[36] analyzed

5

the problem of macrosegregation in a vertical directionally solidified ingot and showed that even subtle temperature gradients in the radial direction can cause considerable macrosegregation in Pb-Sn dendritic alloys at 1 g_0 (g_0 = 9.8 m·s⁻¹).

In none of the above works pertaining to dendritic solidification has the problem of understanding the onset of thermosolutal convection in the all-liquid zone and/or the mushy zone been attempted. Early in the grant period, a related problem of a doubly diffusive system, wherein a porous layer underlies a pool of liquid,[37] was studied. However, in that work solidification phenomena (i.e., moving mushy zone, heat of solidification., etc.) were not included, and the porosity of the porous layer was considered to be constant and uniform. Furthermore, the concentration gradients were not realistic because the advancement of the mushy zone was neglected (i.e., no solidification).

Particularly noteworthy, in combining solidification and convective phenomena in a unified theory, are the publications of Bennon and Incropera who formulated the continuity, momentum, solute and energy equations for solid-liquid mixtures.[38] They used their model to simulate convection and macrosegregation in solidifying aqueous solutions of ammonium chloride.[39,40] Their computations were for horizontal solidification and numerically revealed, for the first time, the formation of channel type "A-segregates."

III. LINEAR STABILITY ANALYSIS OF THERMOSOLUTAL CONVECTION

We consider directional solidification against gravity, as shown in Figure 2. In Figure 2, S denotes the all-solid zone, L is the all-liquid zone, and $L+S$ denotes the two-

phase dendritic region, which is usually called the mushy zone. The mushy zone is treated as a porous medium with a variable porosity. For the nonconvecting state, we assume that the interfaces between the S and the mushy zone and between the mushy zone and L are planar. Gravity acts in the negative z direction.

Figure 3 illustrates the unperturbed solutal and thermal fields in the nonconvecting state that are appropriate for the dendritic solidification of an alloy in a eutectic system. Corresponding to Figure 2, the mushy zone extends from the eutectic isotherm ($z = 0$) to the isotherm along the dendrite tips ($z = z_t$). With the solidification rate, V, less than approximately 0.1 cm·s^{-1}, which is certainly appropriate in most solidification processes of dendritic alloys, we can ignore the effects of curvature at the dendrite tips on both the solutal field and the thermal field in the vicinity of $z = z_t$. Thus, all isotherms and isoconcentrates in the unperturbed state are horizontal. Along the isotherm at the tip of the dendrites, the composition C_t must be slightly greater than the far-field composition C_∞, because there is diffusion in the liquid. Because the Lewis number $\bar{\alpha}/D \gg 1$, the far-field temperature T_∞ is beyond the scale of Figure 3 and is not shown, whereas the far-field concentration is achieved at approximately $z = z_t + D/V$, where D is the solute diffusivity in the liquid and $\bar{\alpha}$ is the thermal diffusivity.

We also make the following assumptions that are common to the forms of the continuity, momentum, energy, and solute conservation equations that we employ:

(1) The mushy zone moves with a constant solidification velocity V (in the z direction), and the overall shape of the mushy zone is constant.

(2) There is no mass diffusion in the solid.

7

(3) Flow is two-dimensional.

(4) The solid and liquid phases have constant and equal densities, ρ.

A. *The Conservation Equations*

Because solidification is considered to be steady, we introduce a coordinate

system that moves with the solidification velocity V. The continuity equation, consistent

with assumptions (3) and (4), is

$$\frac{\partial u}{\partial x} + \frac{\partial w}{\partial z} = 0 \qquad [1]$$

where u and w are the components of the superficial velocity in the x and z directions.

For this work, the solid is stationary, and we have selected the momentum

equation recommended by Beckermann and Viskanta,[41] with the "effective viscosity"

taken to be the reference dynamic viscosity, μ_0, and the density of the liquid to be equal

to the reference density, ρ_0, except for the body force for which we use the Boussinesq

approximation. With these assumptions, the components of the momentum equation are

(x momentum)

$$\frac{\partial u}{\partial t} - V\frac{\partial u}{\partial z} + \frac{1}{\phi}\left[u\frac{\partial u}{\partial x} + w\frac{\partial u}{\partial z}\right] = -\frac{\phi}{\rho_0}\frac{\partial p}{\partial x} + \nu_0\nabla^2 u - \frac{\nu_0\phi}{K}u \qquad [2]$$

(z momentum)

$$\frac{\partial w}{\partial t} - V\frac{\partial w}{\partial z} + \frac{1}{\phi}\left[u\frac{\partial w}{\partial x} + w\frac{\partial w}{\partial z}\right] = -\frac{\phi}{\rho_0}\frac{\partial p}{\partial z} + \nu_0\nabla^2 w - \frac{\nu_0\phi}{K}w - \phi\frac{\rho}{\rho_0}g \qquad [3]$$

8

In Eqs. [2] and [3], K is the permeability, assumed to be isotropic, and ϕ is the volume fraction of liquid. The reference state is the liquid at a temperature T_0 and solute concentration C_0. The formulation subsumes both the Darcian and non-Darcian (Brinkman) terms to account for the porous medium behavior over the entire range of volume fraction of liquid within the mushy zone. It is important to note that in the vicinity of the dendrite tips, use of the Darcian term alone would introduce serious error, whereas by including the Brinkman term, we permit viscous shear. Note that K is a function of ϕ,[42] and K approaches infinity as ϕ approaches 1. The Boussinesq approximation for the buoyancy term is included by the variable density, ρ, which depends on solute concentration and temperature. Finally, v_0 is the kinematic viscosity of the liquid at its reference state (C_0, T_0).

For the energy equation, many additional assumptions are added to those listed above. The added assumptions are the following:

(1) The local temperature of the solid and liquid are equal ($T_s = T_L = T$).

(2) The thermal conduction flux is given by Fourier's rate law for conduction.

(3) The thermal conductivity within the mushy zone can be represented as an effective conductivity, κ.

(4) The latent heat of fusion, L, throughout the solidification temperature range is constant.

(5) It follows from assumption (4) that $dH_S = dH_L = \hat{c}dT$, where H_S and H_L are the intensive enthalpies of the dendritic solid and interdendritic liquid, respectively, and $\hat{c}$ is the heat capacity of the mushy zone.

9

With all of these assumptions, the energy equation can be written as follows:

(energy)

$$\frac{\partial T}{\partial t} + u \frac{\partial T}{\partial x} + (w - V) \frac{\partial T}{\partial z} - \bar{\alpha} \nabla^2 T - \frac{L}{\hat{c}} \frac{\partial \phi}{\partial t} + \frac{VL}{\hat{c}} \frac{\partial \phi}{\partial z} \qquad [4]$$

where $\bar{\alpha} = \kappa / \rho_0 \hat{c}$. In Eq. [4], the usual transient, advection, and conduction terms are represented; the second term on the right-hand side accounts for the evolution of the latent heat of fusion during solidification.

For the solute conservation equation, we use the model of Flemings and Nereo,[2] but with no solidification shrinkage and with constant density. The concentration of solute in the interdendritic liquid is C, and it is tied to the local temperature by equilibrium thermodynamics (i.e., the liquidus of the equilibrium phase diagram). Added to the derivation given by Flemings and Nereo,[2] we include Fickian diffusion of solute in the interdendritic liquid in the direction of the thermal gradient. The final form is

(solute)

$$\phi \frac{\partial C}{\partial t} + u \frac{\partial C}{\partial x} + (w - \phi V) \frac{\partial C}{\partial z} - D \left[\phi \nabla^2 C + \frac{\partial C}{\partial z} \frac{\partial \phi}{\partial z} + \frac{\partial C}{\partial x} \frac{\partial \phi}{\partial x} \right]$$

$$- (1 - k) \frac{\partial \phi}{\partial t} + (1 - k) V \frac{\partial \phi}{\partial z} C \qquad [5]$$

where D is the solute diffusivity in the liquid and k is the equilibrium partition ratio, which is assumed to be constant.

Each of Eqs. [1] through [5] reduces to the usual form for the all-liquid zone as $\phi \rightarrow 1$. Thus, we are assured of continuity between the variables in the mushy zone and the variables in the all-liquid zone.

10

This set of equations requires boundary conditions. They are:

at $z = 0$,

$$T - T_E; \qquad C - C_E; \qquad u - w - 0 \qquad \text{[6a,b,c]}$$

at $z = \infty$ (far-field conditions),

$$C - C_\infty; \qquad T - T_\infty; \qquad u - w - 0 \qquad \text{[7a,b,c]}$$

C_E and T_E are concentration of solute and temperature at the eutectic isotherm, respectively.

We now express the system of equations in perturbed variables and retain only the linear terms. We, therefore, write

$$u - u_s(z) + u'(x,z,t) \qquad \text{[8]}$$

$$w - w_s(z) + w'(x,z,t) \qquad \text{[9]}$$

$$p - p_s(z) + p'(x,z,t) \qquad \text{[10]}$$

$$C - C_s(z) + C'(x,z,t) \qquad \text{[11]}$$

$$T - T_s(z) + T'(x,z,t) \qquad \text{[12]}$$

$$\phi - \phi_s(z) + \phi'(x,z,t) \qquad \text{[13]}$$

where the subscript s indicates the variable in the non-convecting and steady state (i.e., the basic state), and the variables u', w', p', C', T', and ϕ' are the perturbed quantities. Ultimately, for the linear stability analysis, we solve for the perturbed

11

quantities. Of course, by representing the independent variables as Eqs. [8] through [13], it is necessary to describe the basic state.

B. *The Basic State*

By definition of our basic state, $u_s = w_s = 0$, and Eqs. [2] and [3] reduce to

$$\frac{\partial p_s}{\partial x} = 0 \qquad [14]$$

and

$$\frac{dp_s}{dz} = -\rho g \qquad [15]$$

The solute equation for the basic state comes from Eq. [5]. It is

$$\frac{d^2 C_s}{dz^2} + \frac{V}{D}\frac{dC_s}{dz} + \frac{1}{\phi_s}\frac{d\phi_s}{dz}\frac{dC_s}{dz} + \frac{(1-k)V}{\phi_s D}\frac{d\phi_s}{dz}C_s = 0 \qquad [16]$$

The energy equation for the basic state is derived from Eq. [4]. For the mushy zone, it is convenient to write it in terms of concentration, by making use of $m = dT/dC$, which is the slope of the liquidus on the equilibrium phase diagram. The result ($0 \le z \le z_i$) is

$$\frac{d^2 C_s}{dz^2} + \frac{V}{\bar{\alpha}}\frac{dC_s}{dz} + \frac{VL}{m\hat{c}\bar{\alpha}}\frac{d\phi_s}{dz} = 0 \qquad [17]$$

The terms C_s and ϕ_s also satisfy

$$C_s(0) = C_E \qquad [18]$$

$$C_s(z_i) = C_i \qquad [19]$$

12

and

$$\phi_s(z_t) - 1 \qquad [20]$$

Equations [16] through [20] must be solved numerically to obtain $C_s(z)$ and $\phi_s(z)$ within the mushy zone. With $C_s(z)$ known, $T_s(z)$ follows from the liquidus of the equilibrium phase diagram. The value of C_t is determined as part of the solution for concentration in the all-liquid zone.

For the all-liquid zone, C_s and T_s are independent, and well-known analytical relationships for each are available. For $z_t < z < \infty$, Eq. [16] reduces to

$$\frac{d^2C_s}{dz^2} + \frac{V}{D}\frac{dC_s}{dz} - 0 \qquad [21]$$

The boundary conditions accompanying Eq. [21] are Eq. [19] and

$$C_s(\infty) - C_\infty \qquad [22]$$

The solution satisfying Eqs. [19], [21], and [22] is

$$\frac{C_s - C_\infty}{C_t - C_\infty} - \exp\left[-\frac{V}{D}(z - z_t)\right] \qquad [23]$$

In order to evaluate C_t, we recognize that steady state requires

$$(C_t - C_\infty)V - -D\left[\frac{dC_s}{dz}\right]_{z_t} \qquad [24]$$

13

Also, $(dC_s/dz)_{z_t} - G_L/m$, where G_L is defined as the thermal gradient at the tip of the dendrites. Then,

$$C_t - C_\infty + \frac{DG_L}{mV} \qquad [25]$$

Thus, $C_s(z)$ can be determined for the entire field of $0 \leq z \leq \infty$. Equation [25] is valid, provided curvature effects at the dendrite tips are negligible.

The temperature in the all-liquid zone for the basic state is readily obtained from Eq. [4]. It is

$$\frac{d^2T_s}{dz^2} + \frac{V}{\bar{\alpha}}\frac{dT_s}{dz} - 0 \qquad [26]$$

The initial conditions for this second-order equation are

$$\left(\frac{dT_s}{dz}\right)_{z_t} - G_L \qquad [27]$$

and

$$T_s(z_t) - T_t \qquad [28]$$

Condition [27] is used because it is convenient to specify G_L as a parameter. The solution that satisfies Eqs. [26] through [28] is

$$T_s - T_t + G_L\frac{\bar{\alpha}}{V}\exp\left[-\frac{V}{\bar{\alpha}}(z - z_t)\right] \qquad [29]$$

14

Thus, $T_s(z)$ can be determined for the entire field of $0 \leq z \leq \infty$.

C. *The Perturbed Variables*

In addition to the six perturbed dependent variables given in Eqs. [8] through [13], it is convenient to define two other perturbed variables. They are

$$\frac{\phi}{K} = \left[\frac{\phi}{K}\right]_s + \left[\frac{\phi}{K}\right]' \qquad [30]$$

and

$$\rho = \rho_s + \rho' \qquad [31]$$

where, as before, s denotes the basic state, and the variables with primes are the perturbed quantities. In reality, this does not add two more dependent variables to the problem, because $K = K(\phi)$ and $\rho = \rho(C,T)$.

To obtain differential equations for the perturbed quantities, the definitions given by Eqs. [8] through [13] and [30] and [31] are substituted into the differential equations for continuity, x and z momentum, energy, and solute conservation. For a linear stability analysis, the inertial terms in Eqs. [2] and [3] and products of perturbed quantities are neglected. In the usual manner, the basic state equations are subtracted from these equations. The result of carrying out these operations gives the set of equations for the perturbed quantities. These equations and the details of the derivation can be found in Nandapurkar et al.[43]

The far-field conditions for the perturbed variables are

$$T'(\infty,t) = 0 \qquad [32]$$

15

$$C'(\infty, t) = 0 \qquad\qquad [33]$$

$$w'(\infty, t) = \frac{\partial w'}{\partial z}(\infty, t) = 0 \qquad\qquad [34]$$

and the conditions at the eutectic isotherm are

$$T'(0, t) = 0 \qquad\qquad [35]$$

$$C'(0, t) = 0 \qquad\qquad [36]$$

and

$$w'(\infty, t) = \frac{\partial w'}{\partial z}(0, t) = 0 \qquad\qquad [37]$$

Equation [37] is applicable for relatively low volume fractions of liquid (e.g., less than 0.4) for which the permeability is quite low, so that the perturbed velocity can be ignored.

The factor $(\phi/K)_s$ can be evaluated for the mushy zone with a columnar dendritic structure[42] by

$$\left[\frac{\phi}{K}\right]_s = \left[\frac{1}{ad_1^2}\right]\left[\frac{1 - \phi_s}{\phi_s^2}\right] \qquad\qquad [38]$$

where d_1 is the primary dendrite arm spacing and a is a constant.

The evaluation of the perturbed density, ρ', is accomplished by recognizing that $\rho = \rho(C, T)$, so

$$\rho' = \frac{\partial \rho}{\partial C} C' + \frac{\partial \rho}{\partial T} T$$

16

with

$$\frac{\partial \rho}{\partial C} = -\rho_0 \beta_C$$

and

$$\frac{\partial \rho}{\partial T} = -\rho_0 \beta_T$$

where β_C and β_T are the solutal and thermal expansion coefficients, respectively.

Therefore,

$$\rho' = -\rho_0 \left[\beta_C C' + \beta_T T' \right] \qquad [39]$$

Further, in the mushy zone, where T and C are linked by the equilibrium phase diagram, $m = T'/C'$, and $\beta_T = \beta_C/m$.

The perturbation equations were simplified by assuming that $\phi = \phi(z)$, where $\phi(z) = \phi_s$. This makes the numerical solution more tractable, yet maintaining the essential ingredient that the stability of the system can be evaluated by perturbing velocity, concentration, and temperature.

With the assumption that $\phi' = 0$, it is convenient to treat the all-liquid zone and the mushy zone individually and couple them by requiring continuity of the variables and their derivatives at $z = z_t$ (i.e., at the tip of dendrites). The set of equations for the perturbed quantities in the all-liquid zone are simply those used for the mushy zone with $\phi_s = 1$ and $[\phi/K]_s = 0$. Boundary conditions, at $z = \infty$ and $z = 0$, for the perturbed variables are given by Eqs. [32] through [34] and Eqs. [35] through [37], respectively.

The perturbed variables are represented in the usual manner:

$$w' = \hat{W}(z)e^{\sigma t + i\omega x} \qquad [40]$$

$$C' = \hat{C}(z)e^{\sigma t + i\omega x} \qquad [41]$$

$$T' = \hat{T}(z)e^{\sigma t + i\omega x} \qquad [42]$$

Here, σ is the temporal growth rate, and ω is the horizontal wave number of the perturbation. By substituting Eqs. [40] through [42] into the conservation equations for the perturbed variables, there results a set of equations for which eigenvalues of σ satisfy the solution. Derivations and the numerical procedures for determining the eigenvalues are given in Nandapurkar et al.[43]

To verify the correctness of this methodology, we used it to solve the eigenvalue problem studied by Coriell et al. (Eqs. 62 through 66 and 70 through 78 in Reference 25) for the case of the directional solidification of an alloy with a planar interface. We solved their disturbance equations using our finite difference code, while Coriell et al. used a shooting method to obtain the neutral stability curves. In addition, we solved their problem by two different approaches. In one, we assumed that the principle of exchange of stabilities holds, set $\sigma = 0$ and computed C_∞ as the eigenvalue. In the other, we treated σ as the eigenvalue and iterated on C_∞ to obtain the onset of instability [$Re(\sigma) = 0$]. Our computed results compared well to the results of Coriell et al.[25] so we have confidence in the numerical techniques.

18

D. *Marginal Stability Curves*

Marginal stability curves were calculated for Pb-20 wt pct Sn alloy, for various fractions of the gravitational constant. Results are shown in Figures 4 through 7. The regions identified with S and U represent regions in which the basic nonconvecting states are stable and unstable, respectively. The calculations were performed for temperature gradients ranging between 0.5 and 100 $K \cdot cm^{-1}$.

For a gravitational constant of 1 g_0 (g_0 = 9.8 $m \cdot s^{-2}$), there are two branches that define the marginal stability of the system (Figure 4). These curves do not exhibit a region where the system is unconditionally stable for all wave numbers, so unless the horizontal width of the container holding the solidifying alloy is quite narrow, convection is expected. However, it would be possible to suppress convection by effecting solidification in narrow molds. For example, with G_L = 10 $K \cdot cm^{-1}$, the system is stable with respect to perturbations with wavelengths less than 0.066 cm. Thus, in molds f widths less than approximately 0.66 mm, there would be no convection during solidification.

Figure 5 gives the marginal stability curves for the gravitational constant of 0.5 g_0. Although the nature of the curves here is qualitatively similar to that at 1 g_0, it is quite clear that the region of instability is compressed, as expected. The calculations indicate that for this situation, the system would be convectively stable in molds of widths less than 0.95 mm for a temperature gradient of 10 $K \cdot cm^{-1}$.

The marginal stability curves change dramatically with a further reduction in the gravitational constant. With the gravitational constant equal to 0.1 g_0 (Figure 6), the system is not unconditionally stable for any specific value of the thermal gradient. But

solidification in wider molds can be accomplished without convection. For example, for a gradient of 2 $K \cdot cm^{-1}$, and in molds less than 0.4-cm wide, solidification without convection is predicted. Also, for gradients greater than about 2.5 $K \cdot m^{-1}$, the system is always stable convectively.

When the gravitational constant is $10^{-2} g_0$, the system exhibits two branches (Figure 7). The marginal stability branch, drawn with the solid curve, is for stationary convection; the region to the left of the broken curve is unstable with respect to oscillatory convection. At the reduced level of the gravitational constant, the system is stable provided $G_L > 0.75$ $K \cdot cm^{-1}$ and the wave numbers are greater than approximately 3.0 cm^{-1}. Thus, no convection is predicted for solidification in molds less than 2.0 cm in width at $10^{-2} g_0$ for all gradients greater than 0.75 $K \cdot cm^{-1}$. It should be mentioned here that when the wave numbers are sufficiently small, the wavelength of the perturbation ($\lambda = 2\pi/\omega \cong z$) has the same order of magnitude as the dimension of the domain, and the assumption of infinitesimality of the perturbations does not hold.

Finally, the linear stability calculations for a gravitational constant of $10^{-4} g_0$ showed that the system is stable for all wave numbers, at least for the range of thermal gradients analyzed (viz., $G_L \geq 2.5$ $K \cdot cm^{-1}$).

E. *Discussion*

When analyzing the stability of a solidifying dendritic alloy, the interaction of the convection in the all-liquid zone and the convection in the mushy zone must be considered. The analysis of the stability of such an interaction, however, appears to be quite complex, in that the marginal stability curves exhibit no minima which would define

20

conditions for which the system is unconditionally stable. Further, if an attempt is made to describe the stability of the system in terms of the usual thermal and solutal Rayleigh numbers, it becomes apparent that these dimensionless parameters are not independent. Thus, one cannot impose a constant stabilizing thermal Rayleigh number and study the stability of the system as a function of a destabilizing solutal Rayleigh number. Unfortunately, this limits the utility of our results to the specific cases considered herein. Of course, the same methodology could be applied to other alloys and solidification conditions.

Despite the complex interaction in solidifying dendritic alloys, the conditions for marginal stability can be studied in terms of dimensional variables. Such analyses are particularly useful in suggesting lateral dimensions of the container that can be used to suppress convection at various values of the gravitational constant. Of course, the system studied herein was unbounded laterally, so it could be argued that the linear stability analysis does not define lateral dimensions to suppress convection. This is true in a precise sense; nevertheless, nonlinear calculations of the convecting system confirm the predictions of the linear stability analyses.[49] Furthermore, as mentioned by McFadden et al.,[28] the inclusion of the effect of sidewalls in the linear stability analysis for thermosolutal convection would make the solution to the problem "intractable, if not impossible." However, Guerin et al.[44] state that for the modified problem of predicting the onset of convection during directional solidification with a planar interface, the presence of the sidewalls is stabilizing. On the basis of their work, we believe that our computed results for the onset of convection are conservative (i.e., when our analysis

21

predicts a motionless state, sidewalls would make the system even more stable with respect to convection).

One assumption in our analysis is that the density of the solid equals that of the liquid. With unequal densities, there would be a flow toward or away from the solid-melt interface. In other words, the basic state would not be motionless, with $u_s = 0$ and $w_s = -\varepsilon V$, where ε is the shrinkage. However, because the value of ε is small, approximately 0.04 for the Pb-Sn alloys analyzed herein, the results would not be significantly affected by relaxing this particular assumption.

Finally, it should be repeated that the volume fraction of liquid, ϕ, has not been perturbed. In a linear analysis, we believe that this is not necessary and is analogous to decoupling the morphological stability of the interface from the convective instabilities that can occur in solidification with a planar interface.

IV. ANALYSIS OF NONLINEAR CONVECTION

In the previous chapter, the thermosolutal convection was analyzed in terms of its linear stability. In this chapter, the same type of a system is formulated using dimensionless variables, and the supercritical convection is calculated.

It is important to note that the present nonlinear analysis does not permit the volume fraction of liquid in the mushy zone to deviate from its distribution determined for the nonconvecting and steady state. While this is a reasonable assumption to make for convection near the critical state, and it permits a prediction of the conditions in which thermosolutal convection is expected, such an assumption probably does not allow an investigation of the supercritical stage of convection that leads to the formation of

localized segregates that are sometimes called "channel segregates" or "freckles."[45] In future work, we intend to model the supercritical convection and the formation of channel segregates by relaxing the assumption that the volume fraction of liquid in the mushy zone does not vary with time.

A. *Dimensionless Conservation Equations*

The physical situation is illustrated by Figure 2. We assume that a binary alloy solidifies vertically in a two-dimensional strip of width W. The coordinate system is located at $z = 0$ and moves upward at the constant solidification velocity, V.

In the previous chapter, all of the major assumptions are listed. The dimensional conservations equations, written for the moving coordinate system are given by Eqs. [1] through [5]. We now rewrite Eqs. [1] through [5] with nondimensional quantities.

(1)   The thermal Rayleigh number is

$$Ra_T = \frac{g\beta_T G_L H^4}{v_0 \bar{\alpha}}$$

where G_L is the specified initial thermal gradient at the tip of the dendrites and H is a characteristic length. For these nonlinear calculations, we have selected $H = z_n$, the height of the mushy zone.

(2) The solutal Rayleigh number is

$$Ra_C = \frac{g\beta_C C_\infty H^3}{v_0 D}$$

where C_∞ is the concentration of solute in the bulk liquid.

(3) The Prandtl number is

$$Pr = v_0 / \bar{\alpha}$$

(4) The Schmidt number is

$$Sc = v_0 / D$$

(5) The Darcy number is

$$Da = K/H^2$$

(6) The reference velocity is

$$U = \left(g\beta_T G_L H^2\right)^{1/2}$$

(7) The nondimensional interface velocity is

$$\hat{V} = V/U$$

The momentum diffusion time scale

$$\tau = \frac{H^2}{v_0}$$

has been chosen because it lies between the temperature and solute diffusion time scales. The temperature and solute concentrations are nondimensionalized according to

$$T - \frac{T' - T_0}{G_L H}$$

and

$$C - \frac{C' - C_\infty}{C_\infty}$$

respectively, where the prime denotes a dimensional quantity and T_0 is the liquidus temperature of the alloy with concentration C_∞. For reference pressure, we choose

$$P - \rho_0 H^2 / \tau^2 \,.$$

Finally, the nondimensional components of velocity are

$$u - u'/U \quad \text{and} \quad w - w'/U$$

The nondimensional coordinates are

$$x - x'/H \quad \text{and} \quad z - z'/H$$

Nondimensional time is

$$t - t'/\tau$$

And nondimensional pressure is

$$p - p*/P$$

Notice that in the definition of the nondimensional pressure, a dimensional pressure p^* is introduced. The dimensional pressure gradient in Eqs. [1] and [2] is written as $\nabla p' = \nabla p_s + \nabla p^*$, where $\nabla p_s = -\rho_0 g$, so that p^* satisfies $\nabla p^* = \nabla p' + \rho_0 g$.

Because the equations in the mushy zone reduce to the equations in the liquid when $\phi = 1$, the whole system can be described by one set of equations. In nondimensional form, Eqs. [1] through [5] become

$$\frac{\partial u}{\partial x} + \frac{\partial w}{\partial z} = 0 \tag{43}$$

$$\frac{\partial u}{\partial t} + \left[\frac{Ra_T}{Pr}\right]^{1/2} \left[\left(\frac{w}{\phi} - \hat{V}\right)\frac{\partial u}{\partial z} + \frac{u}{\phi}\frac{\partial u}{\partial x}\right] = -\phi\left[\frac{Pr}{Ra_T}\right]^{1/2}\frac{\partial p}{\partial x} + \nabla^2 u - \frac{\phi}{Da}u \tag{44}$$

$$\frac{\partial w}{\partial t} + \left[\frac{Ra_T}{Pr}\right]^{1/2} \left[\left(\frac{w}{\phi} - \hat{V}\right)\frac{\partial w}{\partial z} + \frac{u}{\phi}\frac{\partial w}{\partial x}\right] = -\phi\left[\frac{Pr}{Ra_T}\right]^{1/2}\frac{\partial p}{\partial z} + \nabla^2 w - \frac{\phi}{Da}w$$

$$+ \phi\left[\frac{Ra_T}{Pr}\right]^{1/2}\left[T + \frac{Ra_c Pr C}{Ra_T Sc}\right] \tag{45}$$

$$\frac{\partial T}{\partial t} + \left[\frac{Ra_T}{Pr}\right]^{1/2}\left\{u\frac{\partial T}{\partial x} + (w - \hat{V})\frac{\partial T}{\partial z}\right\} = \frac{1}{Pr}\nabla^2 T + \left[\frac{Ra_T}{Pr}\right]^{1/2}\frac{\hat{V}L}{\hat{c}G_L H}\frac{d\phi}{dz} \tag{46}$$

26

$$\phi \frac{\partial C}{\partial t} + \left[\frac{Ra_T}{Pr}\right]^{1/2} \left[u \frac{\partial C}{\partial x} + (w - \phi \hat{V}) \frac{\partial C}{\partial z}\right] - \frac{1}{Sc}\left[\phi \nabla^2 C + \frac{\partial C}{\partial z} \frac{d\phi}{dz}\right]$$

$$+ \left[\frac{Ra_T}{Pr}\right]^{1/2} \hat{V}(1 - k)\frac{d\phi}{dz}(1 + C) \qquad [47]$$

B. *The Initial State*

We assume that initially there is no convection and that, in the mushy zone, Eqs. [16] through [20] of Nandapurkar et al.[43] describe C, T, and ϕ. The nonconvecting state is specified by inputting, G_L, V, and C_∞ with

$$\phi(x, z_t, 0) = 1$$

$$\phi(x, 0, 0) \geq 0$$

and

$$T'(x, 0, 0) = T'_E$$

In addition to obtaining C, T, and ϕ in the nonconvecting mushy zone, the position of the dendrite tips, z_t, is also obtained as part of the solution.

The characteristic length, H, is made equal to z_t, and the height of the all-liquid zone is also made equal to $H = z_t$. The temperature at the top of the all-liquid zone simply becomes

$$T'_H = T'_t + G_L H$$

27

where T'_t is the temperature at the dendrite tips. Thus, within the numerical domain, the temperature gradient in the liquid of the initial state is assumed to be linear. Notice that this initial state does not exactly match the steady-state thermal field, which is strictly obtainable only for an all-liquid zone of infinite height. Because we seek a nonlinear calculation for T, C, u, and w, it is not necessary that the initial state must match a steady state. However, we choose the values of C, T, and ϕ that rigorously match a steady state for the initial condition of the mushy zone.

C. Boundary Conditions

The domain is made finite by means of an artificial top boundary at $z' = z_t + H = 2H$ and by considering only the region $0 \leq z \leq 2H$.

The boundary condition associated with Eqs. [24] through [27] are as follows:

(1) No slip condition on velocities along the two vertical walls and the bottom boundary.

(2) No surface tractions at the top open boundary $z' = 2H$.

$$\sigma \cdot n - 0$$

where n is the unit normal vector pointing outward from the boundary surface.

(3) Adiabatic vertical walls.

(4) Prescribed temperatures at bottom and top boundaries (with $z_t = H$):

$$T(x,0,t) - \frac{T_E - T_0}{G_L H} \quad \text{and} \quad T(x,2H,t) - \frac{T_t - T_0}{G_L H} + 1$$

(5) No solute flux at the vertical and bottom boundaries.

(6) At the top boundary, the solute must balance the concentration C_∞ outside, viz., at the top boundary,

$$\frac{1}{Sc}\frac{\partial C}{\partial z} + \sqrt{\frac{Ra}{Pr}} \, \vec{V}C = 0$$

(7) At the bottom, $z = 0$,

$$C - \frac{C_E - C_\infty}{C_\infty}$$

D. Calculated Results for Nonlinear Convection

The numerical model uses a finite-element code that is described in Heinrich[46] and Heinrich and Yu.[47] The detailed aspects of the method pertaining to a related solidification process can be found in Heinrich,[48] and the strategy for selecting a nonuniform nodal spacing in the z-direction can be found in Heinrich et al.[49]

Calculations were performed for lead-tin systems under a variety of conditions. All calculations were started by introducing a random perturbation in the initial solutal field at the nodal points of the form

$$C(x,z,0) - C_0(z)(1 + 0.005r)$$

where $C_0(z)$ is the solutal concentration of the initial state and $-1 \leq r \leq 1$, with r taken from a random number generator.

First we discuss the results of nonlinear calculations for the Pb-20 wt pct Sn alloy. Table I shows the different cases considered and the results of the linear stability analysis. The solidification velocity is 7.2 cm·h^{-1} (2×10^{-3} cm·s^{-1}) in all cases, and the upper boundary was chosen at $z' = 2H$.

Table I. Calculations for Pb-20 Wt Pct Sn

Calc. No.	Reference Thermal Gradient G_L (K·cm^{-1})	g/g_0 ($g_0 = 980$ cm·s^{-2})	Container Width (cm)	Linear Stability
1	80	1	1.24	unstable
2	80	10^{-4}	1.24	stable
3	2.5	1	3.46	unstable
4	2.5	10^{-1}	3.46	unstable
5	2.5	10^{-2}	3.46	unstable
6	2.5	10^{-4}	3.46	stable
7	2.5	1	0.10	stable

In the case of $G_L = 80$ K·cm^{-1}, the depth of the dendritic region was found to be 1.24 cm, and when the gravitational constant is $g_0 = 980$ cm·s^{-2}, the non-dimensional parameters are $Ra_T = 4.24 \times 10^4$, $Ra_C = 2.33 \times 10^7$, $Pr = 1.58 \times 10^{-2}$, $Sc = 91.0$, and $Da = 6.15 \times 10^{-8} \phi^3/(1 - \phi)$.

All of our nonlinear calculations agree with the linear stability results in the sense that when the stability analysis predicts an unstable case, convection develops in the nonlinear system, and when a stable system is predicted, the perturbations die out in the

nonlinear model. In Figure 8, the results for calculations 1 after 114 seconds are shown. It can be observed that convection is very weak in the all-liquid region, and there is essentially no convection in the mushy zone. In fact, the permeabilities used in these calculations yield almost no convection in the mushy zone in all cases.

In the case G_L = 2.5 K·cm^{-1}, a depth of 17.3 cm results for the mushy zone, and at normal gravity conditions, the nondimensional parameters are Ra_T = 4.97 x 10^7, Ra_C = 6.28 x 10^{10}, Da = 2.75 x 10$^{-9}\phi^3/(1 - \phi)$ with the same values as before for the Prandtl and Schmidt numbers. Results at t = 1080 s for calculations 3 and 5 in Table I are shown in Figures 9 and 10, respectively. As expected, much weaker convection is observed in Figure 10 and Figure 9 because of the reduced value of g. It can be observed that the convection cells in Figure 9 are much longer than those in Figure 8 because of the weaker stabilizing temperature gradient. These calculations show the expected results as predicted by the linear stability analysis of Nandapurkar et al.[43] However, these cases show no convection in the mushy zone and hardly any effect of thermosolutal convection in the conditions at the dendrite tips. We should point out that the linear stability calculations were done for laterally unbounded systems[43] and for values of g sufficiently high to cause convection. The systems were never found to be stable unconditionally for all wavelengths. Therefore, we have assumed that a system is stable provided that the linear analysis predicts stability for wavelengths equal to or greater than the width of the container.

Another series of calculations was performed for a Pb-10 wt pct Sn alloy at G_L = 50 K·cm^{-1} and a lower solidification velocity of 2.5 cm·h^{-1} (approximately 7 x 10^{-4} cm·s^{-1}). These are summarized in Table II.

31

Table II. Calculations for Pb-10 Wt Pct Sn

Calculation Number	Container Width (H = 2.4 cm)	g/g_0 (g_0 = 980 cm·s^{-2})	Linear Stability[5]
8	H	1	unstable
9	$2H$	1	unstable
10	$H/2$	1	unstable
11	$H/4$	1	unstable
12	$H/8$	1	unstable
13	$H/16$	1	stable
14	H	10^{-4}	stable

The results for calculations 8 through 12 confirmed that the size of the convection cells was independent of the width of the container. The depth of the mushy zone was H = 2.4 cm, and the top boundary was chosen at z = $2H$. The parameters for these calculations, when the gravitational constant is g_0, are Ra_T = 6.15 x 10^5, Ra_C = 9.49 x 10^7, Pr = 1.96 x 10^{-2}, Sc = 82.3, and Da = 3.947 x $10^{-7}\phi^3/(1 - \phi)$.

Results for calculation 8 in Table II are shown in Figure 11 at t = 700 s. It can be observed that, in this case, there is significant convection in the upper part of the mushy zone, and convection produces a strong disturbance in the concentration field at the tip of the dendrites. The temperature field remains virtually undisturbed. Note that dimensionless temperature is defined differently and given in the caption. Figure 12 shows a magnification close to the dendrite tips at 1887 seconds. A better organized cell system can be observed at this later time, and the effect of convection in the upper part of the dendrite region is evident. The temperature field has been magnified 100 times and shows how weakly it is affected by convection due to the very low Prandtl number. In all calculations performed so far, using values generally accepted for the Darcy

number, convection in the mushy zone is only significant in the upper 20 pct of the dendrite region, if there is any convection at all. Furthermore, as can be observed in Figure 12(a), convection in the mushy zone is almost entirely driven by convection in the all-liquid region. This is more clearly illustrated by calculation 12 in Table II, for which the detail of the flow in the vicinity of the dendrite tips is depicted in Figure 13 at 1890 seconds. In all these figures, we should keep in mind that the streamline patterns obtained are not unique; they depend on the initial perturbations, and, hence, only the qualitative features of the flows are significant.

Further computations have been performed for this system for the parameters of calculation 8 in Table II but with the gravitational vector oriented slightly off the negative vertical direction. Results show that very small deviations off the vertical direction produce a system entirely dominated by natural convection. The effect of both thermosolutal and natural convection could only be observed for deviations of up to 0.01 deg off the vertical direction. For a slightly larger angle of 0.05 deg, natural convection completely dominated the flow. These results have been reported elsewhere.[50]

E. *Discussion*

Under the simplifying assumptions of steady-state solidification and that the tips of the dendrites describe a plane undeformable surface that advances at a constant velocity, nonlinear calculations of thermosolutal convection during vertical solidification of dendritic alloys have been performed. The model is an extension of the plane-front model analyzed by Coriell et al.[25] and McFadden et al.[51] to include a dendritic zone.

The analysis shows significant differences when compared with the plane-front interface models, because of the presence of the mushy zone, in that the systems can be stable for higher solutal concentration values and were stable for all cases studied at a reduced gravity of $10^{-4} g_0$. This suggests that the plane-front model is not relevant to solidification in the presence of a mushy zone.

The nonlinear calculations are in full agreement with the linear stability analysis presented in Nandapurkar et al.[43] and show that the presence of the mushy zone can have a stabilizing effect and suppress convection under low gravity conditions or when the lateral dimensions of the container are properly chosen. When the system is unstable, "fingerlike" convection develops in the all-liquid region that can entrain the interdendritic liquid in the mushy zone and significantly affect the solute concentration in the neighborhood of the tips of the dendrites. Furthermore, the calculated convection in the mushy zone under these conditions is always weak and very sensitive to the choice of the permeability function. For the permeability models used in this work, convection in the mushy zone never reached further than the upper 20 pct of the mushy zone and appeared to be driven mainly by convection in the all-liquid region.

It was also concluded that at gravity levels of $10^{-4} g_0$, the Pb-Sn alloys considered were always stable to thermosolutal convection; moreover, when gravity is not acting exactly vertically, the presence of natural convection fully dominates the dynamics of the flow, under the conditions of this model.

The model presented here is only valid at the onset of convection. After some time, constitutional equilibrium is not satisfied, because it is assumed that the distribution of the volume fraction liquid remains constant with time. For this reason,

calculations have been performed for a short time after the onset of convection that describe the main qualitative features of the dynamics of the flow in the vicinity of the dendrite tips. Extension of the present model to relax the condition--that the volumetric fraction of interdendritic liquid in the mushy zone is constant--is currently being pursued with the expectation that it will allow us to model the severe localized segregates in which remelting must take place, known as "channel segregates" or "freckles."

V. OTHER ACCOMPLISHMENTS

The major emphasis of the research was to model thermosolutal convection during solidification of dendritic alloys, and the results of this effort are given in Chapters III and IV. In this chapter, we summarize several other tasks of the subject research. For the sake of brevity details are not given here, but the many publications resulting from the work may be consulted.[37,52-69]

A. *Thermal and Salt-Finger Convection in Superposed Fluid and Porous Layers*

When a fluid layer is overlying a porous layer, and fluid in both layers participate in the convection process, the nature and characteristics of the convection are quite different from those occurring in each layer separately. In directional solidification of binary alloys, there is a mushy zone between the solid region and the all-liquid zone. Then convection involves both the mushy zone and the all-liquid zone. Of course, in this instance, an additional important constraint is the thermodynamics of the phase change occurring in the mushy zone. However, in this part of our investigation, we assumed that

the solid matrix in the mushy zone is inert (i.e., there is no solidification). In this manner, rather general results can be obtained based on a small set of parameters.

We made a linear stability analysis of the onset of thermal and salt-fingering convection in the superposed layers. The results show that the presence of the fluid layer drastically alters the onset conditions for convection.[37,52] When the thickness of the fluid layer is larger than approximately 15% of the porous layer thickness, convection is dominated by the fluid layer. When the fluid layer thickness is smaller than 15% of the porous layer thickness, convection is dominated by the porous layer. The sizes of convection cells in these two cases are drastically different. The prediction of the stability theory was confirmed by experiment for the thermal convection case.[53]

A nonlinear computation was carried out by Dr. Falin Chen, as part of his Ph.D. dissertation.[54] The results show that heat transfer is greatly enhanced as the Rayleigh number is increased when convection is porous layer dominated. When the convection is dominated by the fluid layer, the increase of heat transfer with increasing Rayleigh number is rather minimal. Calculations were carried out into the super critical regime up to 20 times the critical Rayleigh number. The convection remains steady, and oscillations were observed.

In directional solidification, the solid in the mushy zone is columnar-dendritic, so that the mushy zone is a porous medium with anisotropic properties, especially in permeability and in heat conductivity. We have recently concluded a linear stability analysis of onset of thermal convection in a superposed fluid and anisotropic porous layers, and a paper entitled "Convective Instability in Superposed Fluid and

Anisotropic Porous Layers" by F. Chen and C. F. Chen has been submitted to *Physics of Fluids*. The abstract of the paper is presented below.

"The onset of thermal convection due to heating from below in a combined system consisting of a fluid layer overlying a porous layer whose permeability and thermal diffusivity may be anisotropic is studied. The flow in the porous medium is assumed to be governed by the Darcy equation, and the Beavers-Joseph condition is applied at the interface between the fluid and porous layers. The linearized stability equations, together with the boundary conditions, are solved by a hybrid Adams and backward difference method. The numerical scheme is first tested for the case in which the depth ratio $\zeta = 10^{-4}$, where ζ is the ratio of the thickness of the fluid layer to that of the porous layer. The results agree with an exact solution for a pure porous layer to three significant figures. Numerical results have been obtained to study the effect of the depth ratio ζ, the degree of anisotropy in permeability ξ (= the ratio of the permeability in the horizontal direction to that in the vertical direction), and the degree of anisotropy in thermal diffusivity ξ_T (= the ratio of thermal diffusivity in the horizontal direction to that in the vertical direction) on the onset of thermal convection. It is found that anisotropy of the porous medium has the most profound effect on the onset of thermal convection when the depth ratio is small. At $\zeta = 0.1$, the critical Rayleigh number increases as ξ is decreased from 1.0 to 0.1 at a given value of ξ_T. This is in accordance with the $\zeta = 0$ case. However, when ξ is decreased beyond the critical value of 0.06, the critical Rayleigh number decreases with decreasing ξ and there is a sudden increase in the critical wavenumber a_m. This sudden change is the result of switching from convection dominated by the porous layer to that dominated by the fluid layer. This

result is illustrated by streamline plots of the pertinent case. For depth ratios $\varsigma \geq 0.2$, convection is confined within the fluid layer at onset so that the effect of anisotropy becomes less important as the depth ratio is increased."

B. *Experimental Study of Directional Solidification of Aqueous Ammonium Chloride Solutions*

Systematic experiments on directional solidification of NH_4Cl-H_2O solutions were carried out to provide ground-based support for the flight experiment "Casting and Solidification Technology" CAST with principal investigators M. H. McCay and T. D. McCay of UTSI. A detailed examination of the onset of plume convection in the mushy layer was made by varying the bottom temperature of the tank, in which the solution solidified. The results are reported in a paper entitled "Experimental Study of Directional Solidification of Aqueous Ammonium Chloride Solutions" by C. F. Chen and F. Chen, which has been submitted to the *Journal of Fluid Mechanics.* The abstract for this paper is presented below.

"Directional solidification experiments have been carried out using the analog casting system of NH_4Cl-H_2O solution by cooling it from below with a constant temperature surface ranging from -31.5°C to +11.9°C. The NH_4Cl concentration was 26% in all solutions, with a liquidus temperature of 15°C. It was found that finger convection occurred in the fluid region right above the mushy layer in all experiments. Plume convection with associated chimneys in the mush occurred in experiments with bottom temperatures as high as +11.0°C. However, when the bottom temperature was raised to +11.9°C, no plume convection was observed, although finger convection was carrying on as usual. A method has been devised to determine the porosity of the mush

38

by computed tomography. Using the mean value of the porosity across the mush layer and the permeability calculated by the Kozeny-Carman relationship, the critical solute Rayleigh number across the mush layer for onset of plume convection was estimated to be between 200 and 250".

## C. *Double-Diffusive Convection under Reduced Gravity*

In a paper to appear,[55] we reported on the effect of reduced gravity on all forms of double-diffusive convection. Using property values of lead-tin alloys, it is concluded that diffusive instability, whether due to sideways heating or bottom heating, is not likely to occur at reduced gravity levels of 10^{-2} to 10^{-4} g_0, where g_0 is the gravitational acceleration at sea level. Salt-finger convection, however, is likely to be generated at much reduced gravity levels. This is because the destabilizing effect of the concentration gradient is amplified by the Lewis number (the ration of thermal diffusivity to solute diffusivity). This has been discussed in depth in a recent AIAA paper.[56] There is a possibility of interaction between salt-finger convection and convection due to surface tension gradients when material processing is being carried out in space. Further studies need to be carried out (a) to delineate the parameter range in which such combined instability may occur and (b) to determine the nature of such convection motions.

D. *Formation of Microporosity during Dendritic Solidification*

A model for the formation of microporosity was included because it is based largely on the description of solute redistribution in the mushy zone that is one of the important facets in our models. Porosity is a defect faced by casting engineers, so it was

felt that our contribution could be useful to the casting community. The transfer of these results was by seminar presentations at an industrial laboratory and a university, talks at three conferences, and four publications.[57-60]

Early in the program Al-4.5 wt pct Cu alloy was chosen as a sample alloy. Calculations were done for various concentrations of dissolved hydrogen. By calculating the partitioning of both hydrogen and copper between the solid and liquid phases in the mushy-zone, the concentration of dissolved hydrogen in the interdendritic liquid during solidification could be calculated. In turn, this concentration is used to determine the pressure of hydrogen gas in the interdendritic liquid according to the following reaction:

$$2\,\underline{H} \to H_2(g)$$
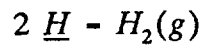
where the underline represents hydrogen in the dissolved state. The equilibrium constant K for the above reaction is

$$K = P_g / C_H^2 \tag{48}$$

where

p_g = pressure of H_2, and

C_H = concentration of dissolved $\underline{H}$ in the interdendritic liquid.

Also

$$K = K(T, C_{cu}) \tag{49}$$

where

T = temperature, and

C_{cu} = concentration of copper in the interdendritic liquid.

C_H, C_{Cu} and T throughout the mushy zone are calculated during solidification, so that P_g can be estimated via Eqs. [2] and [3]. Finally, with a knowledge of the surface tension (liquid/vapor interface) of the alloy and space available for potential gas-bubbles within the interdendritic liquid, the code can be used to predict the formation of interdendritic porosity, and ultimately the volume fraction of interdendritic porosity after solidification is complete.

The procedure, briefly described above, was included in the computer-code and used to make a number of calculations for the volume fraction of interdendritic porosity. Calculated results agreed favorably with data found in the literature.[57,58]

E. Transport and Thermodynamic Properties

Another important task was to select and organize data for the various quantitative models. In particular, data for the densities of the dendritic solid and interdendritic liquid, as well as the densities of the eutectic-solid and eutectic-liquid, have been reviewed and carefully extrapolated to the solidification temperature range of Pb-Sn alloys[61] and aluminum-rich Al-Cu alloys.[62] We also did a careful evaluation of the enthalpies of the phases during solidification of Pb-Sn alloys.[63] For the model which predicts porosity, a simplified theory for the surface tension of melts of binary alloys was developed,[64-66] which was very useful in extrapolating the surface tension data to the solidification range. Finally, because of our treatment of enthalpy during solidification, we discovered that the heat of mixing effect in alloys can be important in modelling solidification phenomena. In this regard, a paper pertaining to directional dendritic solidification[67] and another on morphological stability[68] were published.

41

In connection with separately supported work on the solidification of binary alloys, we estimated the temperature and composition dependence of the viscosity for Al-Cu alloys,[69] using a relationship based on Andrade's viscosity equation.

V. REFERENCES

1. J.S. Kirkaldy and W.V. Youdelis: *Trans. AIME*, 1958, v. 212, pp. 833-40.

2. M.C. Flemings and G.E. Nereo: *Trans. Met. Soc.-AIME*, 1967, v. 239, pp. 1449-61.

3. M.C. Flemings, R. Mehrabian and G.E. Nereo: *Trans. Met. Soc.-AIME*, 1968, v. 242, pp. 41-9.

4. M.C. Flemings and G.E. Nereo: *Trans. Met. Soc.-AIME*, 1968, v. 242, pp. 50-5.

5. R. Mehrabian, M. Keane and M.C. Flemings: *Metall. Trans.*, 1970, v. 1, pp. 1209-20.

6. R. Mehrabian, M. Keane and M.C. Flemings: *Metall. Trans.*, 1970, v. 1, pp. 3238-41.

7. S. Kou, D.R. Poirier and M.C. Flemings: *Electric Furnace Proceedings*, vol. 35, pp. 221-8, Iron and Steel Society of AIME, New York, 1977.

8. S. Kou, D.R. Poirier and M.C. Flemings: *Met. Trans. B*, 1978, vol. 9B, pp. 711-9.

9. S.D. Ridder, F.C. Reyes, S. Chakravorty, R. Mehrabian, J.D. Naumann, J.H. Chen and H.J. Klein: *Met. Trans. B*, 1978, vol. 9B, pp. 415-25.

10. T. Fujii, D.R. Poirier and M.C. Flemings: *Met. Trans. B*, 1979, vol. 10B, pp. 331-9.

11. D. Petrakis, M.C. Flemings and D.R. Poirier: *Modeling of Casting and Welding Processes* (H.D. Brody and D. Apelian, eds.), pp. 285-312, TMS-AIME, Warrendale, PA, 1981.

12. C. Jeanfills, J.H. Chen and H.J. Klein: ibid., pp. 285-312.

13. S. Ridder, S. Kou and R. Mehrabian: *Metall. Trans. B*, 1981, vol. 12B, pp. 435-47.

14. A.L. Maples and D.R. Poirier: *Metall. Trans. B*, 1984, vol. 15B, pp. 163-72.

15. D.R. Poirier, S. Kou, T. Fujii and M.C. Flemings: *Electroslag Remelting*, Report No. AMMRC TR 78-28, Army Materials and Mechanics Research Center, Watertown, MA, June, 1978.

16. D.R. Poirier, M.C. Flemings, R. Mehrabian and H.J. Klein: *Advances in Metal Processing* (J.J. Burke, R. Mehrabian, V. Weiss, eds.), pp. 277-318, Plenum Publishing, New York, 1981.

17. S.M. Copley, A.F. Giamei, S.M. Johnson and M.F. Hornbecker: *Metall. Trans.*, 1970, vol. 1, pp. 2193-2204.

18. M.E. Glicksman, S.R. Coriell and G.B. McFadden: *Ann. Rev. Fluid Mech.*, 1986, vol. 18, pp. 307-35.

19. S.R. Coriell, G.B. McFadden and R.F. Sekerka: *Ann Rev. Mater. Sci.*, 1985, vol. 15, pp. 119-45.

20. W.A. Tiller, K.A. Jackson, J.W. Rutter and B. Chalmers: *Acta. Metall.*, 1953, vol. 1, pp. 428-37.

21. W.W. Mullins and R.F. Sekerka: *J. Appl. Phys.*, 1964, vol. 35, pp. 444-52.

22. M.C. Flemings: *Solidification Processing*, 1974, McGraw-Hill.

23. W. Kurz and D.J. Fisher: *Fundamentals of Solidification*, 1986, Trans. Tech. Publications.

24. J.S. Langer: *Mat. Sci. Eng.*, 1984, vol. 65, pp. 37-44.

25. S.R. Coriell, M.R. Cordes, W. Boettinger and R.F. Sekerka: *J. Cryst. Growth*, 1980, vol. 49, pp. 13-28.

26. S.R. Coriell, G.B. McFadden, R.F. Boisvert and R.F. Sekerka: *J. Cryst. Growth*, 1984, vol. 69, pp. 15-22.

27. K. Brattkus and S.M. Davis: *J. Cryst. Growth*, 1988, vol. 87, pp. 385-96.

28. G.B. McFadden, S.R. Coriell and R.F. Boisvert: *Phys. Fluids*, 1985, 28(9), pp. 2716-22.

29. J.S. Turner: *Ann. Rev. Fluid Mech.*, 1985, vol. 17, pp. 11-24.

30. A.F. Giamei and B.H. Kear: *Metall. Trans.*, 1970, vol. 1, pp. 2185-92.

31. V. Laxmanan, A. Studer, L. Wang, J.F. Wallace and E.A. Winsa: "Gravitational Macrosegregation in Binary Pb-Sn Alloy Ingots", NASA Technical Memorandum 89885.

32. A.K. Sample and A. Hellawell: *Metall. Trans. A*, 1984, vol. 15A, pp. 2163-73.

33. R.N. Hills, D.E. Loper and P.H. Roberts: *Q.J. Mech. Appl. Math.*, 1983, vol. 36, pp. 505-39.

34. H.E. Huppert and M.G. Worster: *Nature*, 1985, vol. 314, pp. 703-07.

35. M.G. Worster: *J. Fluid Mech.*, 1986, vol. 167, pp. 481-501.

36. K.S. Yeum and D.R. Poirier: *Cast Metals*, 1988, vol. 1, pp. 161-170.

37. F. Chen and C.F. Chen: *Trans. ASME, J. Heat Transfer*, 1988. vol. 110, pp. 403-9.

38. W.D. Bennon and F.P. Incropera: *Int. J. Heat Mass Transfer*, 1987, vol. 30, pp. 2161-70.

39. W.D. Bennon and F.P. Incropera: *Int. J. Heat Mass Transfer*, 1987, vol. 30, pp. 2171-87.

40. W.D. Bennon and F.P. Incropera: *Metall. Trans. B*, 1987, vol. 18B, pp. 611-7.

41. C. Beckermann and R. Viskanta: *Int. J. Heat Mass Transfer*, 1988, vol. 31, pp. 35-46.

42. D.R. Poirier: *Metall. Trans. B*, 1987, vol. 18B, pp. 245-55.

43. P. Nandapurkar, D.R. Poirier, J.C. Heinrich and S. Felicelli: *Metall. Trans. B*, 1989, vol. 20B, pp. 711-21.

44. R.Z. Guerin, B. Billia, P. Maldenwang and B. Roux: *Phys. Fluids*, 1988, vol. 31, pp. 2086-92.

45. J.R. Sarazin and A. Hellawell: *Metall. Trans. B*, 1988, vol. 19B, pp. 1861-71.

46. J.C. Heinrich: *Int. J. Numer. Meth. Eng.*, 1984, vol. 20, pp. 447-64.

47. J.C. Heinrich and C.-C. Yu: *Comput. Meth. Appl. Mech. Eng.*, 1988, vol. 69, pp. 1-27.

48. J.C. Heinrich: *Comput. Meth. Appl. Mech. Eng.*, 1988, vol. 69, pp. 65-88.

49. J.C. Heinrich, S. Felicelli, P. Nandapurkar and D.R. Poirier: *Metall. Trans. B*, 1989, vol. 20B, pp. 883-91.

50. J.C. Heinrich, S. Felicelli, P. Nandapurkar and D.R. Poirier: Paper No. 89-0626, 27th AIAA Aerospace Science Meeting, Reno, NV, Jan. 8-12, 1988.

51. G.B. McFadden, R.G. Rehm, S.R. Coriell, W. Chuch and K.A. Morrish: *Metall. Trans. A*, 1984, vol. 15A, pp. 2125-37.

52. F. Chen: *Trans. ASME, J. Heat Transfer*, 1990, to appear.

53. F. Chen and C.F. Chen: *J. Fluid Mech.*, 1989, vol. 207, pp. 311-21.

54. F. Chen: Ph.D. Dissertation, Dept. of Aerospace and Mechanical Engineering, The University of Arizona, Tucson, AZ, 1989.

55. C.F. Chen: "Double-Diffusive Convection and Its Effects under Reduced Gravity," in *Progress in Low-Gravity Fluid Dynamics and Transport Phenomena*, J.N. Koster and R. Sani, editors, AIAA, Washington, D.C., 1990, to appear.

56. C.F. Chen: Paper No. 90-0122, 29th AIAA Aerospace Science Meeting, Reno, NV, Jan. 8-11, 1990. Will appear in *Microgravity and Space Processing Symposium Proceedings*.

57. D.R. Poirier, K. Yeum and A.L. Maples: *Metall. Trans. B*, 1987, vol. 18B, pp. 1979-87.

58. D.R. Poirier and K. Yeum: *Proceedings of Solidification Processing 1987*, Sheffield, U.K., Sept. 21-24, 1987, pp. 8-10.

59. D.R. Poirier and K. Yeum: *Proceedings of the 35th Annual Meeting of the Inestment Casting Institute*, Washington, D.C., Oct. 5-7, 1987, pp. 11:1-33.

60. K. Yeum and D.R. Poirier: *Light Metals 1988*, AIME, Warrendale, PA, 1988, pp. 469-76.

61. D.R. Poirier: *Metall. Trans. A*, 1988, vol. 19A, pp. 2349-54.

62. S. Ganesan and D.R. Poirier: *Metall. Trans. A*, 1987, vol. 18A, pp. 721-3.

63. D.R. Poirier and P. Nandapurkar: *Metall. Trans. A*, 1988, vol. 19A, pp. 3057-61.

64. D.R. Poirier and R. Speiser: *Metall. Trans. A*, 1987, vol. 18A, 1987, pp. 1156-60.

65. K. Yeum, R. Speiser and D.R. Poirier: *Scripta Metall.*, 1987, vol. 21, pp. 687-92.

66. K.S. Yeum, R. Speiser and D.R. Poirier: *Metall. Trans. B*, 1989, vol. 20B, pp. 693-703.

67. K.S. Yeum and D.R. Poirier: *Cast Metals*, 1988, vol. 1, pp. 161-70.

68. P. Nandapurkar and D.R. Poirier: *J. Crystal Growth*, 1988, vol. 92, pp. 88-96.

69. S. Ganesan, R. Speiser and D.R. Poirier: *Metall. Trans. B*, 1987, vol. 18B, pp. 421-4.
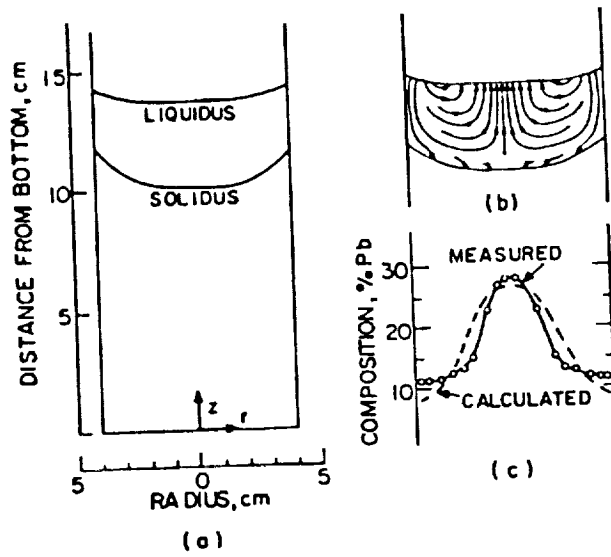
Fig. 1--Interdendritic fluid flow and macrosegregation in an ingot of Sn-15 wt pct Pb. (a) liquidus and solidus isotherms; (b) flow lines of interdendritic liquid, (c) macrosegregation. From Kou et al.[7]
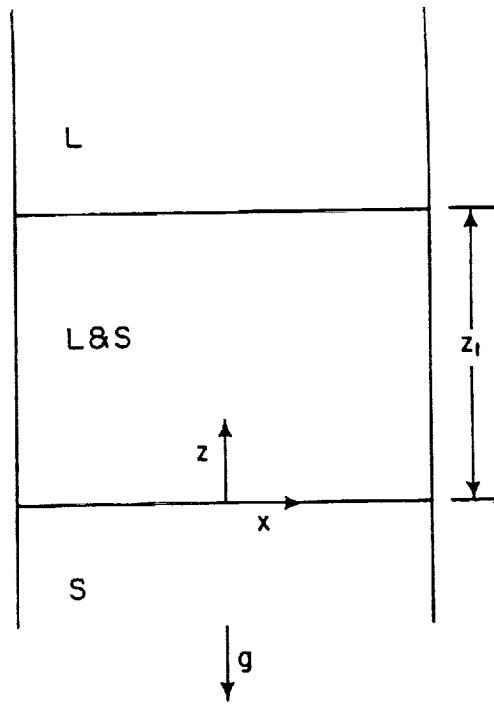
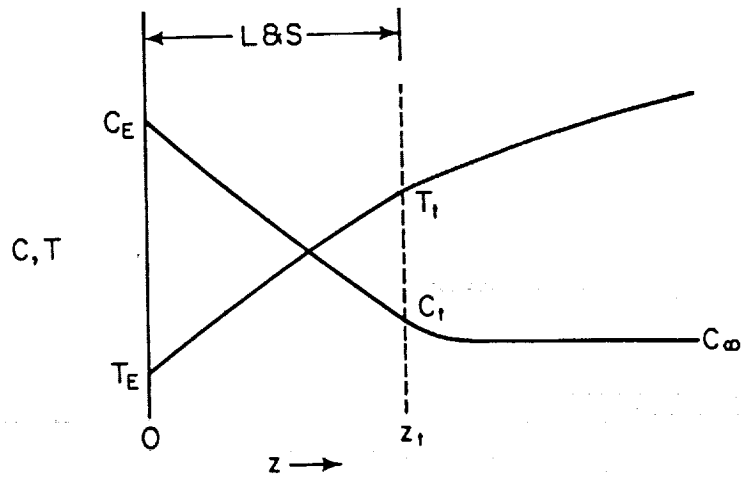Fig. 2--Directional solidification of a dendritic alloy with a mushy zone of depth z_t.

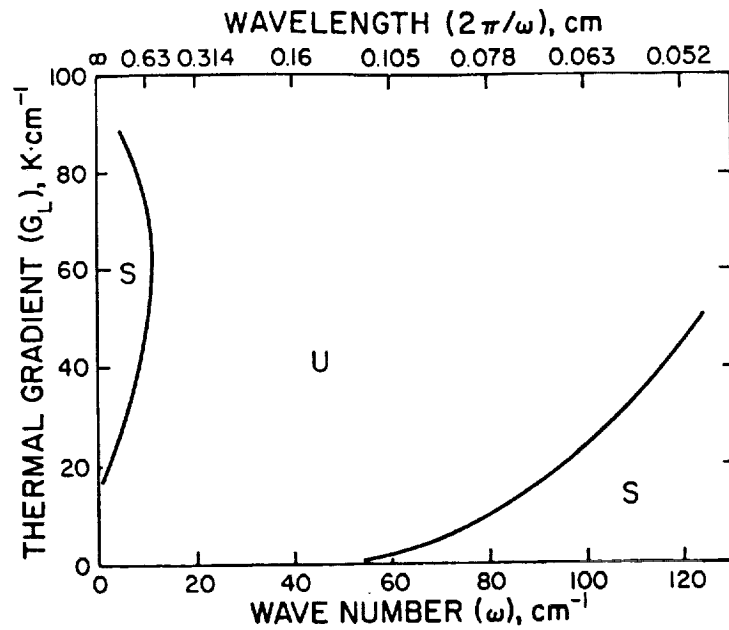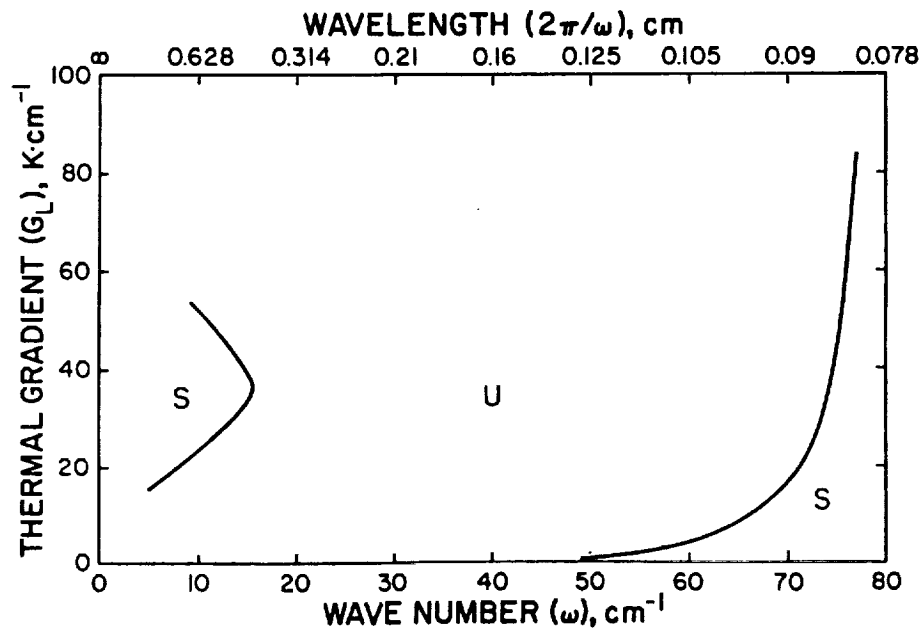Fig. 3--Solutal and thermal fields for the directional solidification of a dendritic alloy.

Fig. 4--Marginal stability curves for the dendritic solidification of Pb-20 wt pct Sn for a solidification rate of 2×10^{-3} cm·s^{-1} with a gravitational constant of $1\ g_0$. Stationary convection is predicted in the region U.
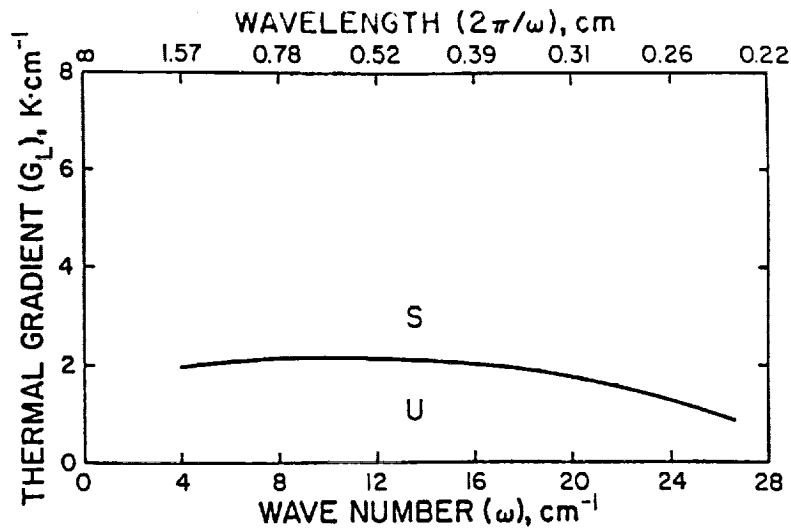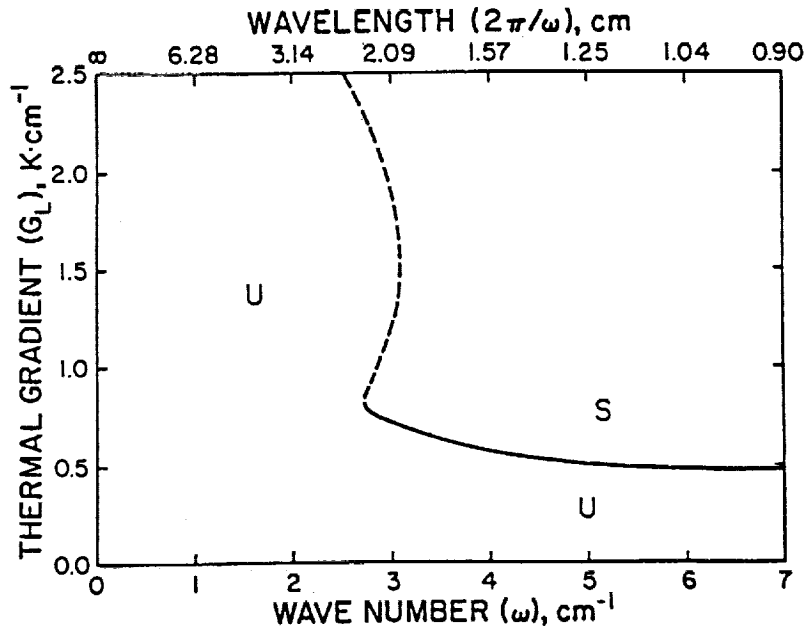

Fig. 5--Marginal stability curves for the dendritic solidification of Pb-20 wt pct Sn for a solidification rate of 2×10^{-3} cm·s^{-1} with a gravitational constant of $0.5\ g_0$. Stationary convection is predicted in the region U.

Fig. 6--Marginal stability curves for the dendritic solidification of Pb-20 wt pct Sn for a solidification rate of 2 x 10^{-3} cm·s^{-1} with a gravitational constant of 0.1 g_0. Stationary convection is predicted in the region U.

Fig. 7--Marginal stability curves for the dendritic solidification of Pb-20 wt pct Sn for a solidification rate of 2 x 10^{-3} cm·s^{-1} with a gravitational constant of 0.01 g_0. The region U under the solid curve is for stationary and the region U to the left of the broken curve is for oscillatory convection.
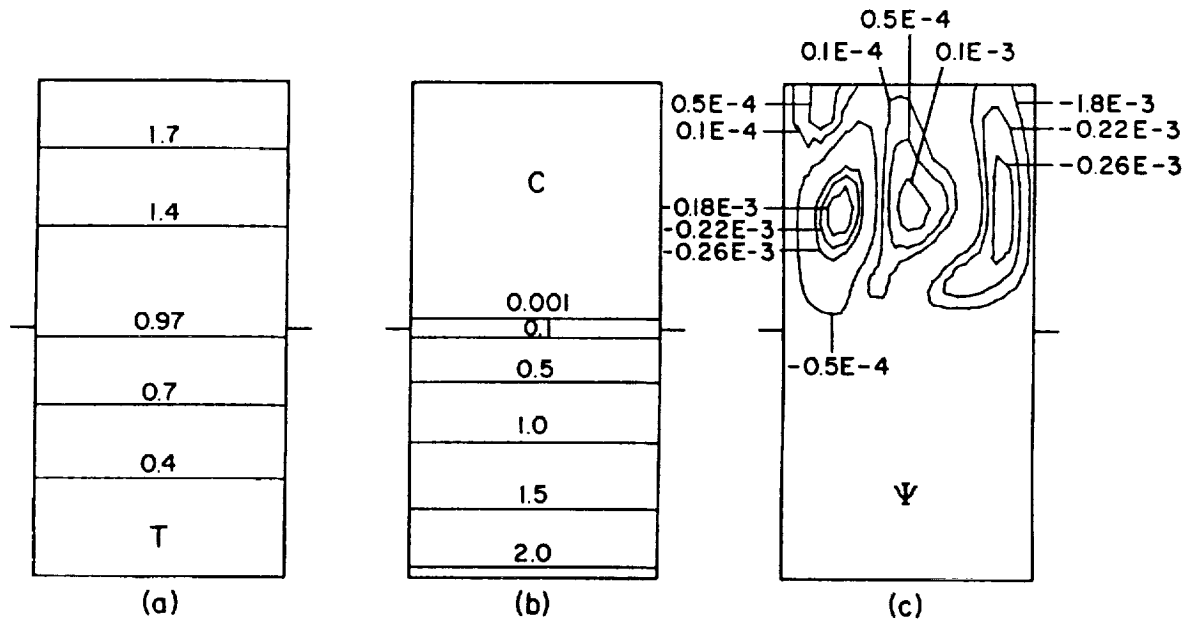
Fig. 8--Convection in a Pb-20 wt pct Sn alloy (calculation 1) at 114 s with $G_L = 80$ K·cm^{-1}. (a) Isotherms are $(T' - T_E)/(T_t - T_E)$, (b) solutal isoconcentrates, and (c) streamline contours.

(a)
3.0
T
2.6
2.3
1.4
0.7

(b)
C
0.001
0.1
0.5
1.0
1.5
2.0

(c)
−0.2E−2
−0.3E−2
−0.4E−2
0.2E−3
0.6E−3
−0.1E−2
−0.2E−2
−0.3E−2
0.1E−2
0.6E−3
0.2E−3
Ψ
0.2E−3
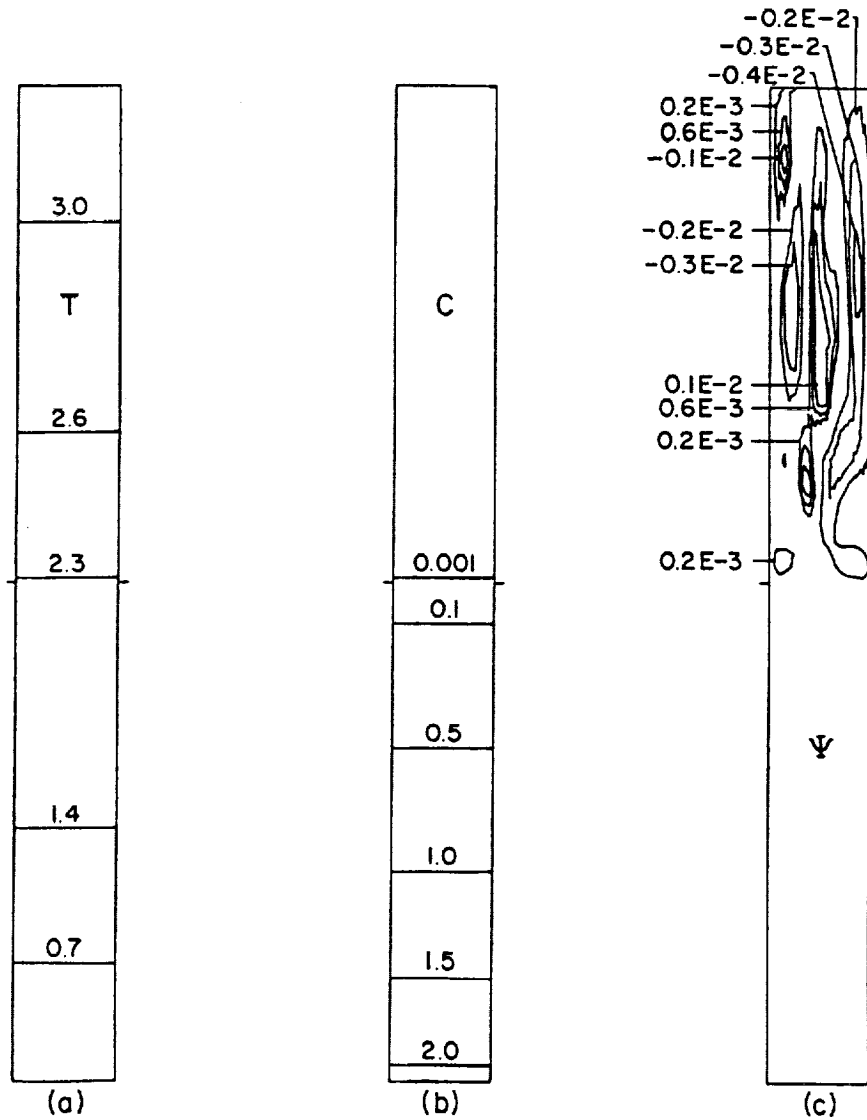
Fig. 9--Convection in a Pb-20 wt pct Sn alloy (calculation 3) at 1080 s with $G_L = 2.5$ K·cm^{-1}. (a) Isotherms are $(T' - T_E)/(T_t - T_E)$, (b) solutal isoconcentrates, and (c) streamline contours.

(a)

3.0

T

2.6

2.3

1.4

0.7

(b)

C

0.001
0.1
0.5
1.0
1.5
2.0

(c)

0.1E-4
0.7E-4
0.2E-3
-0.9E-4
-0.2E-3

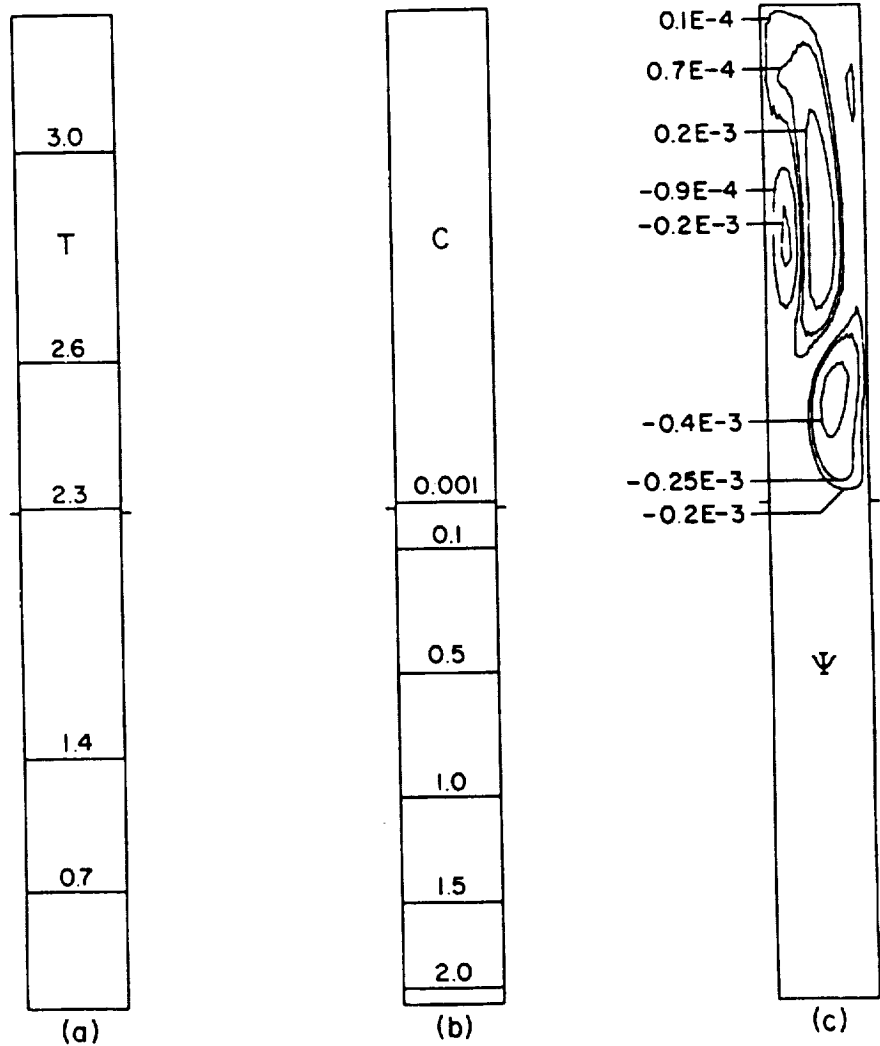-0.4E-3
-0.25E-3
-0.2E-3

Ψ

Fig. 10--Convection in a Pb-20 wt pct Sn alloy of Fig. 9 but at the reduced gravity 0.01 g_0 (calculation 5). (a) Isotherms are $(T' - T_E)/(T_t - T_E)$, (b) solutal isoconcentrates, and (c) streamline contours.

NASA Report Documentation Page

| 1. Report No.
NASA CR - 187078	2. Government Accession No.	3. Recipient's Catalog No.

| 4. Title and Subtitle
The Role of Gravity on Macrosegregation in Alloys | 5. Report Date
March 1991 |
|---|---|
| | 6. Performing Organization Code |

| 7. Author(s)
D.R. Poirier, C.F. Chen, and J.C. Heinrich | 8. Performing Organization Report No.
None |
|---|---|
| | 10. Work Unit No.
674 - 25 - 05 |

| 9. Performing Organization Name and Address
The University of Arizona
College of Engineering and Mines
Tucson, Arizona 85721 | 11. Contract or Grant No.
NAG3 - 723 |
|---|---|
| | 13. Type of Report and Period Covered
Contractor Report
Final |
| 12. Sponsoring Agency Name and Address
National Aeronautics and Space Administration
Lewis Research Center
Cleveland, Ohio 44135 - 3191 | 14. Sponsoring Agency Code |

15. Supplementary Notes

Project Manager, Arnon Chait, Materials Division, NASA Lewis Research Center, (216) 433 - 3558.

16. Abstract

During dendritic solidification liquid flow is induced both by buoyancy forces and solidification shrinkage. Based largely on the experimental base of other NASA-sponsored investigators, there is strong evidence that the major reason for the liquid flow is the former, i.e., thermosolutal convection. In the microgravity environment, it is thought that the thermosolutal convection will be greatly diminished so that convection will be confined mainly to the flow of interdendritic liquid required to satisfy the solidification shrinkage. The major motivation for this work has been to provide improved models to the NASA community involved in performing and planning space experiments on dendritic solidification with emphasis on convection and macrosegregation. Another motivation for this work is that macrosegregation is an extremely important subject to the commercial casting community. We believe that work of this type, especially when combined with the experimental results of other NASA-sponsored investigators, will be crucially important in providing a basic understanding of macrosegregation to the casting community. This report describes the simulation of thermosolutal convection in directionally solidified (DS) alloys. A linear stability analysis was used to predict marginal stability curves for a system that comprises a mushy zone underlying an all-liquid zone. In the unperturbed and nonconvecting state (i.e., the basic state), isotherms and isoconcentrates are planar and horizontal. The mushy zone is realistically treated as a medium with a variable volume fraction of liquid that is consistent with the energy and solute conservation equations. The perturbed variables include temperature, concentration of solute, and both components of velocity in a two-dimensional system. As a model system, an alloy of Pb-20 wt pct Sn, solidifying at a velocity of 2×10^{-3} cm·s^{-1}, was selected. Dimensional numerical calculations were done to define the marginal stability curves in terms of the thermal gradient at the dendrite tips, G_L, vs the horizontal wave number of the perturbed quantities. For a gravitational constant of $0.01g_0 \le g \le g_0$ ($g_0 = 9.8$ cm·s^{-2}), the marginal stability curves show no minima; thus, the system is never unconditionally stable. Nevertheless, such calculations quantify the effect of reducing the gravitational constant on reducing convection and suggest lateral dimensions of the mold for the purpose of suppressing convection. Finally, for a gravitational constant of $10^{-4}g_0$, calculations show that the system is stable for the thermal gradients investigated ($2.5 \le G_L \le 100$ K·cm^{-1}). The supercritical thermosolutal convection in directionally solidified dendritic alloys was also modeled. The model assumes a nonconvective initial state with planar and horizontal isotherms and isoconcentrates that move upward at a constant solidification velocity. The initial state is perturbed, nonlinear calculations are performed to model convection of the liquid when the system is unstable, and the results are compared with the predictions of linear stability analysis. The mushy zone is modeled as a porous medium of variable porosity, consistent with the volume fraction of interdendritic liquid that satisfies the conservation equations of energy and solute concentrations. Results are presented for systems involving lead-tin alloys (Pb-10 wt pct Sn and Pb-20 wt pct Sn) and show significant differences with results of plane-front solidification. The calculations show that convection in the mushy zone is mainly driven by convection in the all-liquid region, and convection of the interdendritic liquid is only significant in the upper 20 percent of the mushy zone if it is significant at all. The calculated results also show that the systems are stable at reduced gravity levels of the order of $10^{-4}g_0$ or when the lateral dimensions of the container are small enough, for stable temperature gradients between $2.5 \le G_L \le 100$ K·cm^{-1} at solidification velocities of 2 to 8 cm·h^{-1}. The linear stability analyses and the calculations of the nonlinear thermosolutal convection can be used to study the dendritic solidification. In addition to those tasks, this report briefly describes analysis and experiments on thermal and salt-finger convection in systems comprising a fluid layer overlying a porous medium. Finally, the aspect of solute redistribution during dendritic solidification was extended in a model to predict the formation of microporosity. Lacking data pertaining to the solidification of alloys, methods to estimate necessary transport and thermodynamic properties were also developed.

| 17. Key Words (Suggested by Author(s))
Microgravity
Solidification
Macrosegregation
Alloy casting | 18. Distribution Statement
Unclassified - Unlimited
Subject Category 26 |
|---|---|

| 19. Security Classif. (of the report)
Unclassified | 20. Security Classif. (of this page)
Unclassified | 21. No. of pages
60 | 22. Price*
A04 |
|---|---|---|---|